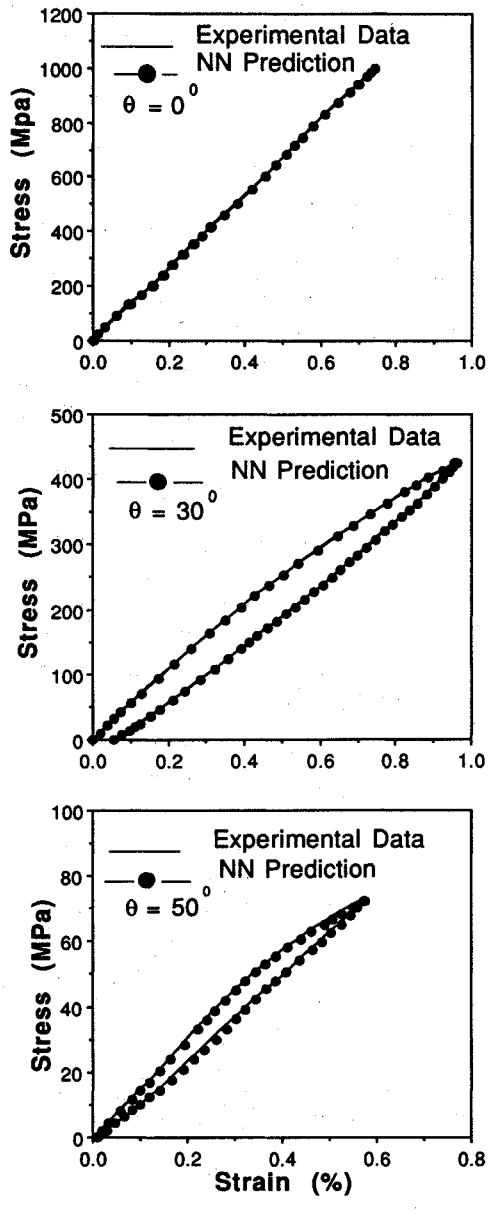

Fig. 3 Comparison of neural network predictions with experimental data for graphite-epoxy (±θ) laminates under cyclic loading for trained data.

nates in the literature, no other predictions are made for the cyclic stress-strain behavior.

Concluding Remarks

Two different back-propagation neural networks were developed to represent the nonlinear stress-strain behavior of (±θ) graphite-epoxy laminates under monotonic and cyclic loadings. The NN predictions for both monotonic and cyclic loadings are in good agreement with the experimental data obtained from the literature. These preliminary results support the use of a NN approach to composite material modeling. The network developed in this study aids in identifying important aspects of the stress-strain behavior, such as breaking stress, fracture stress, etc. This approach can also be used to predict failure mechanisms.

Acknowledgments

The first author thanks P. A. Lagace of MIT for providing the list of papers on graphite-epoxy composites and Moffit Othman for assisting with the neural network experiments. This research was supported by an internal grant from the Faculty Development Office of Indiana University/Purdue University at Indianapolis.

References

[1]Rumelhart, D. E., Hinton, G. E., and McClelland, J. L., "A General Framework for Parallel Distributed Processing," *Parallel Distributed Processing, Vol. I: Foundations,* The MIT Press, Massachusetts, 1986, pp. 45–76.

[2]Rumelhart, D. E., and Zipser, D., "Feature Discovery by Competitive Learning," *Cognitive Science,* Vol. 9, 1985, pp. 75–112.

[3]Handelman, D. A., Lane, S. H., and Gelfand, J. J., "Integrating Neural Networks and Knowledge-Based Systems for Intelligent Robotic Control," *IEEE Control Systems Magazine,* April 1990, pp. 77–86.

[4]Hajela, P., and Berke, L., "Neurobiological Computational Models in Structural Analysis and Design," *Proceedings of 31st AIAA Structures, Structural Dynamics, and Materials Conference,* Huntsville, AL, April 1990, pp. 345–355.

[5]Palakal, M., and Zoran, M. J., "A Neural-Network-Based Learning System for Speech Processing," *Expert Systems with Applications: An International Journal,* Pergamon Press, New York, 1990, pp. 59–71.

[6]Lippmann, R. P., "An Introduction to Computing with Neural Nets," *IEEE, Acoustic, Speech, and Signal Processing Magazine,* Vol. 4, No. 2, 1987, pp. 4–22.

[7]Freeman, J. A., and Skapura, D. M., *Neural Networks: Algorithms, Applications, and Programming Techniques,* Addison Wesley, New York, 1991.

[8]Ghaboussi, J., Garrett, J. H., Jr., and Wu, X., "Knowledge-Based Modeling of Material Behavior with Neural Network," *Proceedings of ASCE, Journal of Engineering Mechanics,* Vol. 117, No. 1, 1991, pp. 132–153.

[9]Lagace, P. A., "Nonlinear Stress-Strain Behavior of Graphite/Epoxy Laminates," *AIAA Journal,* Vol. 23, No. 10, 1985, pp. 1583-1589.

Postbuckling Analysis of Composite Laminated Cylindrical Panels Under Axial Compression

J. H. Kweon* and C. S. Hong†
Korea Advanced Institute of Science and Technology, Kusong-Dong, Yusong-Gu, Taejon 305-701, Korea

Introduction

IN designing shell-type structures, the buckling and postbuckling behaviors have been considered as the important issues. Specifically, the composite cylindrical panel has been an object of great interest in the weight-sensitive structures due to its high specific stiffness and strength.[1–5] Unlike the flat plate, the cylindrical panel has the limit points on the equilibrium path. The limit point and numerical problems related to that have been the obstacles to the postbuckling analysis of cylindrical panels, and a great number of numerical schemes have been proposed to overcome these problems. The most widely used scheme is the arc-length method.[6]

In this Note, the postbuckling behavior of composite laminated cylindrical panels with various stacking sequences under compression is investigated by the nonlinear finite element method. For the finite element analysis, the updated Lagrangian formulation and the eight-node degenerated shell element are used. An improved load-increment method based on the arc-length scheme is proposed for the postbuckling analysis. Experiments are conducted to verify the validity of the present analysis for a cross-ply laminate.

Finite Element Formulation

At an arbitrary $(n + 1)$st equilibrium state, the principle of virtual work is expressed as

$$\iiint_{V^{n+1}} \sigma_{ij}^{n+1} \delta e_{ij}^{n+1} \, dV = \iiint_{V_f^{n+1}} f_i^{n+1} \delta u_i^{n+1} \, dV + \iint_{S_T^{n+1}} T_i^{n+1} \delta u_i^{n+1} \, dS \tag{1}$$

Received Aug. 25, 1992; revision received Feb. 15, 1993; accepted for publication Feb. 28, 1993.

*Research Assistant, Department of Aerospace Engineering.
†Professor, Department of Aerospace Engineering. Member AIAA.

where σ_{ij}, e_{ij}, f_i, T_i, u_i, and δ are the Cauchy stress, infinitesimal strain, body force, surface traction, displacement, and variation operator, respectively.

In the case of no body force, Eq. (1) can be rewritten in terms of the second Piola-Kirchhoff stress S_{ij} and the Green strain ε_{ij} taking the configuration at the nth equilibrium state as the reference one:

$$\iiint_{V^n} (\sigma_{ij} \Delta S_{ij})\, \delta(\Delta \varepsilon_{ij})\, dV - \iint_{S_T^n} (T_i^n + \Delta T_i)\, \delta(\Delta u_i)\, dS = 0 \tag{2}$$

From Eq. (2), the finite element equation for the composite laminated cylindrical panel is derived :

$$[K_T]\, \{\Delta u^{n+1}\} = -\{\Delta P(\lambda^{n+1})\} \tag{3}$$

where

$$[K_T] = \iiint_{V^n} [B_L^n]^T [D^n]\, [B_L^n]\, dV + \iiint_{V^n} [B_{NL}^n]^T [\bar{\sigma}^n]\, [B_{NL}^n]\, dV \tag{4}$$

$$\{\Delta P(\lambda^{n+1})\} = \{R^{n+1}\} - \lambda^{n+1} \{F_o\} \tag{5}$$

$$\{R^{n+1}\} = \iiint_{V^n} [B_L^n]^T \{\sigma^n\}\, dV \tag{6}$$

In Eqs. (4–6), $[B_L]$, $[B_{NL}]$, $\{\sigma\}$, and $[\bar{\sigma}]$ can be found in Ref. 7. Also $[D]$, λ, and $\{F_o\}$ are material stiffness matrix in the global coordinate system, load-parameter, and force-distribution vector, respectively.

The finite element used is the eight-node degenerated shell element, and the first order shear deformation theory is applied to the element. Incremental displacement fields in the element are expressed as

$$\begin{Bmatrix} \Delta u \\ \Delta v \\ \Delta w \end{Bmatrix} = \sum_{n=1}^{8} H_n(\xi, \eta) \begin{Bmatrix} \Delta u_n \\ \Delta v_n \\ \Delta w_n \end{Bmatrix} + \frac{1}{2} \sum_{n=1}^{8} H_n(\xi, \eta) t_n \zeta \{\Delta V_{n\zeta}\} \tag{7}$$

where ξ, η, and ζ are local coordinates of the element. Also, $H_n(\xi, \eta)$, t_n, and $\{\Delta V_n \zeta\}$ are shape function, thickness, and increment of the vector in the direction of ζ, respectively.

Load-Increment Method

The load increment in the arc-length method is accomplished as

$$\Delta\lambda^1 = \pm \Delta l\, [\{u_T\}^T \{u_T\}]^{-1/2}$$

$$\text{with } \{u_T\} = [K_T]^{-1} \{F_o\} \tag{8}$$

In the conventional arc-length schemes, the sign of $\Delta\lambda^1$ is determined according to that of the determinant of the finite element stiffness matrix. However, using this determinant-based load-increment method in the analysis of a quasi-isotropic panel like the $[0/\pm 45/90]_S$ panel, the sign of the determinant oscillates between positive and negative just after the buckling. A similar phenomenon was found in the analysis of the stiffened steel diaphragm in Ref. 6.

In the method proposed in this Note, the direction of the load increment is independent of the determinant of the stiffness matrix, and the condition is imposed that the first incremental displacement vector in the present load step should make an acute angle with the total incremental displacement vector at the last step:

$$\{\Delta_t u_N\}^T \{\Delta u_{N+1}^1\} > 0 \tag{9}$$

Using this criterion for the load increment, numerical problems did not occur in the postbuckling analysis, and the time for the evaluation of the determinant was saved.

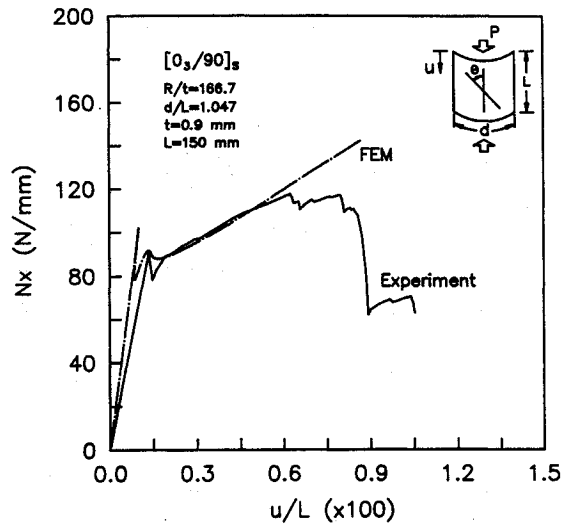

Fig. 1 Finite element and experimental load-shortening curves of the $[0_3/90]_S$ panel.

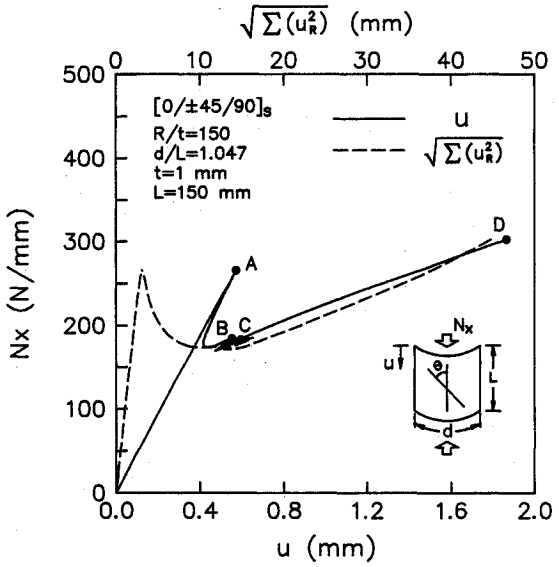

Fig. 2 Load-shortening and load-deflection curves of the $[0/\pm 45/90/]_S$ panel.

Results and Discussion

The stacking sequences considered are unidirectional, angle ply, cross ply, and quasi-isotropic. The fiber angle θ for each layer is defined as the counterclockwise angle from the longitudinal axis of the panel. Boundary conditions are clamped on the curved edges and simply supported along straight edges constraining circumferential displacement. Both the radius of curvature and the panel length are 150 mm. The ratio of panel width to length is 1.047. The panel thickness is 1 mm. The material properties of T300/5208 are used as $E_1 = 181$ GPa, $E_2 = E_3 = 10.3$ GPa, $G_{12} = G_{13} = G_{23} = 7.17$ GPa, and $\nu_{12} = \nu_{13} = \nu_{23} = 0.28$. Also, after the convergence test of element size, the panels without the bending-twisting coupling stiffness are divided by a 5×5 mesh for a quarter of the panel and others are analyzed with 10×10 mesh for the whole panel.

Comparison with Experiment

To verify the validity of the present finite element analysis, experiments were conducted for a $[0_3/90]_S$ panel. For the comparison with experimental results, material properties and panel thickness were used in this case as follows: $E_1 = 130.0$ GPa, $E_2 = E_3 = 10.0$ GPa, $G_{12} = G_{13} = 4.85$ GPa, $G_{23} = 3.62$ GPa, $\nu_{12} = \nu_{13} = 0.31$, $\nu_{23} = 0.52$, and $t = 0.9$ mm. As shown in Fig. 1, the present finite element result is well correlated to the experiment in the buckling

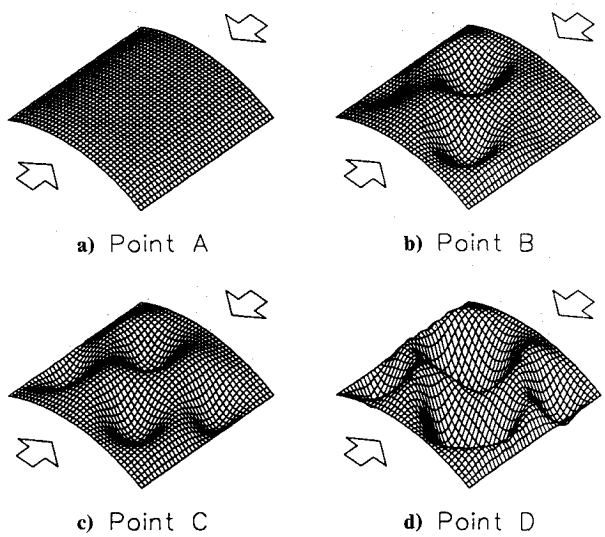

Fig. 3 Three dimensional plots of postbuckling deformed shapes of the $[0/\pm45/90]_S$ panel.

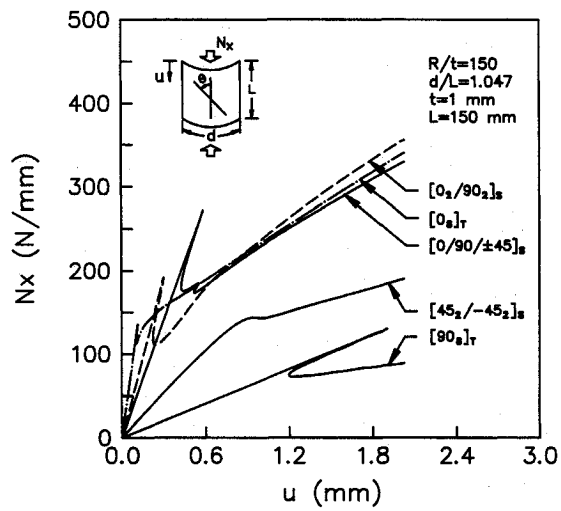

Fig. 4 Equilibrium paths for various laminated cylindrical panels.

and postbuckling load-carrying capacity. It is presumed that a little difference in the buckling loads is due to the imperfections in geometry, material, boundary condition, and alignment. Because the effects of the initial imperfections vanish as the deflection becomes large, the difference in the load-shortening curves is reduced. In this study, since the effect of failure on the stiffness degradation is not considered, the finite element result does not follow the experimental equilibrium path after the failure.

Postbuckling Behavior

Typical load-shortening and load-deflection curves of the $[0/\pm45/90]_S$ panel are shown in Fig. 2. The deflection of the panel is given in terms of the sum of radial displacement u_R at all of the finite element nodes. After the axial load passes the first load-limit point, the axial load and the edge displacement are reduced drastically. The path between the first and second load-limit points is the process that the panel in the unstable equilibrium state is deformed to the stable configuration. When the deformation is developed to the stable equilibrium state, the gradient of the equilibrium path becomes positive and the carried load is increased again. Also, it should be noted that the total deflection is increased even on the path where the edge displacement is reduced. The postbuckling shapes of the panel are shown in Fig. 3. As the deformations are developed progressively, the bending moment about the curved edge is concentrated to the inwardly deformed region. Therefore, the magnitude of deflection is enlarged, and the inwardly deformed regions are extended to the whole panel. Also, the second buckling accompanied by the small load reduction and the change in the deformation shape occurs after the first buckling.

The equilibrium paths for other panels are shown in Fig. 4. The postbuckling load-carrying capacities are different from the initial buckling loads. Whereas the difference between buckling loads of the $[0_8]_T$ and $[90_8]_T$ panels is 3.9%, the postbuckling load-carrying capacity of the $[0_8]_T$ panel is extremely greater than that of the $[90_8]_T$ panel. Although the $[45_2/-45_2]_S$ angle-ply panel has a buckling load higher than that of the $[0_8]_T$ panel, the postbuckling load-carrying capacity is extremely lower than that of the $[0_8]_T$ panel. As the deformations are progressed, the differences in the loads carried by the $[0/90/\pm45]_S$, $[0_2/90_2]_S$, and $[0_8]_T$ panels are decreased. The final load-carrying capacities are rearranged in the order of their magnitude as $[0_2/90_2]_S$, $[0_8]_T$, and $[0/90/\pm45]_S$ panels. This distribution of the postbuckling load-carrying capacities different from that of the initial buckling loads results from the difference in the bending stiffness in the axial direction D_{11}. Because the buckled panel experiences large rotation, the bending moment about the curved edge becomes the dominant loading pattern. Therefore the importance of D_{11} is enlarged in the buckled panel. The $[90_8]_T$ panel cannot resist the bending moment about the curved edge and has the poor load-carrying capacity after the buckling. In contrast with the $[90_8]_T$ panel, the $[0_8]_T$ panel in which the stiffness D_{11} is large shows the small load reduction at the first limit point and has the high load-carrying capacity after the buckling. From present results, it is known that the postbuckling load-carrying capacities of laminated cylindrical panels under compression are largely dependent on the bending stiffness component D_{11}, and not only the buckling loads but also the postbuckling load-carrying capacities should be considered in designing the structure.

Acknowledgment

The experiments in this work were conducted by Research Assistant I. C. Lee.

References

[1]Jun, S. M., and Hong, C. S., "Buckling Behavior of Laminated Composite Cylindrical Panels under Axial Compression," *Computers and Structures*, Vol. 29, No. 3, 1988, pp. 479–490.

[2]Hong, C. S., and Jun, S. M., "Buckling Behavior of Laminated Composite Cylindrical Panel with Initial Imperfections," *Recent Developments in Buckling of Structures*, PVP-Vol. 183, AD-Vol. 18, American Society of Mechanical Engineers, New York, 1989, pp. 9–15.

[3]Sheinman, I., Shaw, D., and Simitses, D. J., "Nonlinear Analysis of Axially-Loaded Laminated Cylindrical Shells," *Computers and Structures*, Vol. 16, No. 1–4, 1983, pp. 131–137.

[4]Snell, M. B., and Morley, N. T., "The Compression Buckling Behavior of Highly Curved Panels of Carbon Fibre Reinforced Plastic," *Proceedings of the 5th International Conference on Composite Materials*, The Metallurgical Society, Warrendale, PA, (San Diego, CA), 1985, pp. 1327–1354.

[5]Knight, N. F., Jr., Starnes, J. H., Jr., and Waters, W. A., Jr., "Postbuckling Behavior of Selected Graphite-Epoxy Cylindrical Panels Loaded in Axial Compression," AIAA Paper 86-0881, May 1986.

[6]Crisfield, M. A., "A Fast Incremental/Iterative Solution Procedure that Handles Snap-Through," *Computers and Structures*, Vol. 13, No. 1–3, 1981, pp. 55–62.

[7]Bathe, K. J., *Finite Element Procedures in Engineering Analysis*, Prentice Hall, Englewood Cliffs, NJ, 1982.